Article

Sunlight-Driven Degradation of Alprazolam and Amitriptyline by Application of Binary Zinc Oxide and Tin Oxide Powders

Nina Finčur [1], Daniela Šojić Merkulov [1,*], Predrag Putnik [2,*], Vesna Despotović [1], Nemanja Banić [1], Szabolcs Bognár [1], Dušica Jovanović [1], Sanja Panić [3], Tamara Ivetić [4] and Biljana Abramović [1]

[1] Department of Chemistry, Biochemistry and Environmental Protection, University of Novi Sad Faculty of Sciences, Trg Dositeja Obradovića 3, 21000 Novi Sad, Serbia; nina.fincur@dh.uns.ac.rs (N.F.); vesna.despotovic@dh.uns.ac.rs (V.D.); nemanja.banic@dh.uns.ac.rs (N.B.); sabolc.bognar@dh.uns.ac.rs (S.B.); dusica.jovanovic@dh.uns.ac.rs (D.J.); biljana.abramovic@dh.uns.ac.rs (B.A.)
[2] Department of Food Technology, University North, Trg Dr. Žarka Dolinara 1, 48000 Koprivnica, Croatia
[3] University of Novi Sad, Faculty of Technology Novi Sad, Bulevar Cara Lazara 1, 21000 Novi Sad, Serbia; sanjar@tf.uns.ac.rs
[4] Department of Physics, University of Novi Sad Faculty of Sciences, Trg Dositeja Obradovića 4, 21000 Novi Sad, Serbia; tamara.ivetic@df.uns.ac.rs
* Correspondence: daniela.sojic@dh.uns.ac.rs (D.Š.M.); pputnik@alumni.uconn.edu (P.P.)

Abstract: In recent years, much attention has been paid to pharmaceuticals as potential toxic bioactive substances in the worldwide environment. These compounds are continuously introduced into the surroundings in small concentrations, which certainly affects the quality of water, ecosystem, and the general health of living organisms. Photocatalysis is a promising technique for treating pharmaceutically active compounds as organic pollutants over traditional technologies. This study proposes the application of photocatalysts composed of zinc oxide (ZnO) and tin oxide (SnO_2), synthesized using a solid-state method, for the photocatalytic degradation of two selected psychoactive drugs, amitriptyline (AMI) and alprazolam (ALP), under simulated solar and UV irradiation in an aqueous system. The newly synthesized photocatalysts were characterized using the following techniques: SEM/EDS, XRD, DLS, and UV/Vis spectroscopy. The obtained data confirmed the successful synthesis and the possible photocatalytic application of the new materials. Concerning the photocatalytic evaluation, the main results indicate that the highest removal efficiency of AMI and ALP was reached in the presence of ZnO/SnO_2 synthesized in a molar ratio of 2:1 and calcined at 700 °C, under 1.0 mg/mL catalyst loading. Based on the reutilization findings, it can be concluded that the mentioned photocatalyst had not lost its efficiency after three successive runs for the photodegradation of ALP. Additionally, pure ZnO powders showed the highest activity after calcination at 500 °C, in the case of both examined pollutants. The experiments with tert-butanol, sodium fluoride, and ethylenediaminetetraacetic acid suggested that the relative contribution of various reactive species changed in the following order: positively charged holes > $OH^{\bullet}_{free}$ > $OH^{\bullet}_{ads}$.

Keywords: psychoactive drug; amitriptyline; alprazolam; photocatalysis; zinc-tin oxide; nanopowders; simulated solar and UV irradiation

1. Introduction

Over the last years, the release of harmful pollutants into the environment, as a result of the massive exploitation of natural resources and widespread use of chemicals, has drawn a lot of attention due to its negative effects on human health [1]. Rapid growth of the population and the number of agricultural and industrial activities have magnified the production of synthetic chemicals, especially in developing countries, and caused the serious global pollution of natural waters. Some of the synthetic organic materials include pharmaceuticals and personal care products. The abundant organic pollutants in surface waters are persistent in the aquatic environments and pose a risk to aquatic organisms upon long-term exposure, even at low concentrations of ng/L [2,3].

Pharmaceutically active compounds have been detected in the environment at low or very low concentrations, where their continuous entry into the environment may lead to prolonged exposure and thus may cause adverse effects on non-targeted organisms. These substances enter the environment mostly as a result of medical and veterinary use [4]. Among those, psychoactive drugs and antidepressants can be used to prevent and reduce the symptoms of depression. As a representative of tricyclic antidepressants, amitriptyline (AMI) inhibits the reuptake of the neurotransmitters noradrenaline and serotonin from the synapses of the central nervous system [5,6]. Benzodiazepines (BZDs) belong to a class of psychoactive drugs that enhance the effect of the neurotransmitter γ-aminobutyric acid, resulting in their use as sedatives and in the treatments of anxiety or amnesia [7,8]. However, BZDs also exhibit some adverse effects on human health, since the long-term consumption of these pharmaceuticals can lead to poisoning and addiction [9]. Alprazolam (ALP) is an anxiolytic that belongs to the new generation of 1,4-benzodiazepines. ALP is most commonly used as an antidepressant but can also be used to treat social phobia and panic disorders [7]. ALP was detected in tap and wastewater at the concentration of ng/L [10]. Due to their low biodegradability, both AMI and ALP are extremely persistent pollutants [8,11]; thus, it is necessary to find a method for their successful removal from the environment.

Wastewater treatment plants are able to remove the majority of pollutants from wastewater. However, some trace organic compounds cannot be degraded by conventional three-step wastewater treatment [12]. Great efforts are being made to find a way to inactivate or eliminate these compounds from surface and wastewater [2,13]. Beside the fact that the ideal wastewater treatment should completely mineralize toxic pollutants with no residual toxic intermediaries left, it also should be cost effective [14]. Among Advanced Oxidation Processes, homogeneous and heterogeneous photocatalytic degradation have stood out as promising techniques for industrial wastewater treatment, as well as in the treatment of underground waters and contaminated air [13]. This process is based on the formation of reactive species of oxygen (e.g., $OH^\bullet$ radicals), which attack the pollutants present. The unlimited source of solar energy, mild reaction conditions, and high efficiency, as the most important advantages of photocatalysis, help to count photocatalysis among the green approaches in water remediation [15].

Metal oxide semiconductors, such as TiO_2, ZnO, and SnO_2, have been the promising choice of researchers for fundamental research and practical applications due to their chemical inertness, high activity, non-toxicity, and low cost. Among various metal-oxide-semiconductors that have been employed as photocatalysts, the application of coupled semiconductors can have a positive effect on the efficiency of photocatalytic degradation and as a consequence of expanding the range of radiation absorption, increasing charge separation, reducing charge recombination, as well as preventing the photocorrosion of semiconductors with a smaller energy gap [16]. Coupled catalysts, such as ZnO/Fe_2O_3, ZnO/WO_3, ZnO/SnO_2, TiO_2/WO_3, TiO_2/SnO_2, and TiO_2/ZnO, often show higher photocatalytic efficiency than individual semiconductors. The controlled synthesis of coupled photocatalysts can also help achieve optimal photocatalytic activity [17]. Besides the abovementioned materials, other heterojunction-based semiconductors, such as 2D/2D $WO_3/BiOBr$, $BiVO_4/BiOBr$, or 2D/2D CoAl-LDH/BiOBr, can also be successfully applied for the removal of various pharmaceuticals from the aqueous environment [18–20]. Furthermore, g-C_3N_4-based or graphene-based materials are also trending topics in photocatalysis [21,22].
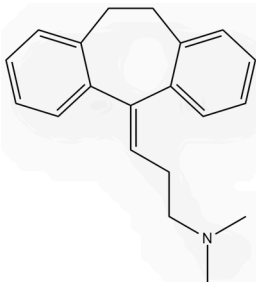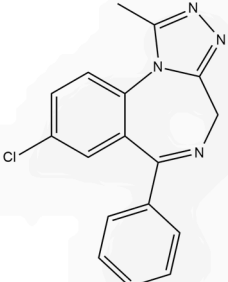
In this study, the photocatalytic efficiency of the coupled ZnO/SnO_2 nanoparticles in the removal of AMI and ALP from an aqueous medium was investigated, using simulated solar irradiation (SSI) and UV irradiation. The influence of the molar ratio of ZnO and SnO_2, the calcination temperature of pure ZnO and coupled photocatalysts, the irradiation type, and photocatalyst loading on the removal efficiency of the mentioned pharmaceutically active components was studied. Moreover, in order to identify the main reactive species involved in the photodegradation process, the effects of various radical and hole scavengers were also examined.

2. Materials and Methods

2.1. Reagents and Chemicals

The nanopowders were prepared from the precursors ZnO and SnO_2 (Sigma-Aldrich, purity 99.9% and particle size $\leq$ 1 mm). The properties of investigated psychoactive drugs are presented in Table 1. AMI (3-(10,11-dihydro-5*H*-dibenzo[*a,d*][7]annulen-5-ylidene)-*N*,*N*-dimethylpropan-1-amine hydrochloride, CAS No. 549-18-8, $\geq$98%) and ALP (8-chloro-1-methyl-6-phenyl-4*H*-[1,2,4]triazole[4,3,-α]-[1,4]-benzodiazepine, CAS No. 28981-97-,7 $\geq$98%) were purchased from Sigma-Aldrich, St. Louis, MO, USA. In addition, tert-butanol (TB) and ethylenediaminetetraacetic acid (EDTA, 99.4–100.6%) were procured form Sigma-Aldrich, St. Louis, MO, USA and sodium fluoride (NaF) was from Alkaloid, Skopje, North Macedonia. All reagents and chemicals were used as supplied without further purification and all aqueous solutions were prepared using ultrapure water.

Table 1. Physicochemical properties of investigated psychoactive drugs, AMI and ALP.

Parameter	AMI	ALP
Chemical structure		
Chemical formula	$C_{20}H_{24}ClN$	$C_{17}H_{13}ClN_4$
Molecular weight (g/mol)	308.7	313.9
Absorption maximum (nm)	206	222
Therapeutic group	tricyclic antidepressant	anxiolytic

2.2. Synthesis and Characterization of Nanopowders

The binary coupled ZnO/SnO_2 nanoparticle powder mixtures were prepared using a solid-state method, where starting precursors (commercially available ZnO, Sigma–Aldrich, purity 99.9% and SnO_2, Sigma–Aldrich, purity 99.99%) were stoichiometrically mixed at both 2:1 and 1:1 molar ratios and mechanically activated for 120 min in a high-energy ball mill (Retsch GmbH PM100) using a zirconia vial and zirconia balls of 10 mm diameter and standard balls at a powder mass ratio of 10:1. Obtained powders were annealed at different temperatures (500, 600, and 700 °C) in air for 120 min and ground again. The ZnO/SnO_2 photocatalysts were labeled as follows: ZnO/SnO_2 (2:1), 500; ZnO/SnO_2 (2:1), 600; ZnO/SnO_2 (2:1), 700; ZnO/SnO_2 (1:1), 500; ZnO/SnO_2 (1:1), 600; ZnO/SnO_2 (1:1), 700. In addition, pure ZnO was annealed at different temperatures (500–1100 °C) and labeled as ZnO 500, ZnO 600, ZnO 700, ZnO 900, and ZnO 1100. Moreover, commercially available TiO_2 Degussa P25 (75% anatase and 25% rutile, average particle size of about 20 nm, according to the producer's specification, specific surface area of 53.2 m^2/g, and total pore volume 0.134 cm^3/g [23]) was used for a comparison of photocatalytic activity. Two samples, ZnO 500 and ZnO/SnO_2 (1:1), 500, were selected for physicochemical characterization, since they showed the highest photocatalytic efficiency in the removal of the selected drugs. The structure and morphology of these nanopowders were characterized with a scanning electron microscope (SEM JEOL JSM-6460LV) coupled with X-ray energy dispersion (EDS). X-ray diffraction (XRD) measurements were performed on a Rigaku Miniflex 600 unit (Cu Kα radiation, λ = 0.15406 nm) using a counting step of 0.3° and a counting time per step of 3 s. The average size of crystallites was obtained using Scherrer's equation. Size distributions of the particles and the zeta potentials were determined with a Zetasizer Nano ZS (Malvern Instruments Ltd., Malvern, UK) based on the DLS technique. Before the measurements, the

samples were dispersed in water and sonicated for 5 min to make them homogeneous. The pH of the prepared solutions was 5. Optical characterization of the samples was performed using a UV–visible spectrometer (CECIL 2021).

2.3. Measurements of Photocatalytic Activity

Each photocatalytic process was carried out as follows: the initial concentration of investigated psychoactive drug (AMI/ALP) was 0.03 mmol/L, while the catalyst loading was 1.0 mg/mL. A weighted amount of photocatalyst was different in experiments where the optimal catalyst loading was investigated (0.1–5.0 mg/mL). In order to obtain insight into the mechanism of photocatalytic degradation of ALP, TB, NaF, and EDTA (1.0 mmol/L) were added to the suspension as scavengers of different reactive species. A cell made of Pyrex glass (total volume of ca. 40 mL) with a plain window for the light beam focus, a magnetic stirring bar, and the water-circulating jacket were used in the photocatalytic degradation experiments. Uniform dispersion with the photocatalyst and adsorption equilibrium was achieved via sonication (Bandelin electronic, high frequency 35 kHz) of the suspension, prior to irradiation in dark for 15 min. It was observed that there was no adsorption under these experimental conditions. The suspension was thermostatted at 25 °C in an O_2 stream (3.0 mL/min). The obtained suspension was then illuminated through SSI using a 50 W halogen lamp (Philips; $\lambda > 380$ nm) with an intensity of 63.85 mW/cm^2 in the visible region and 218.8 μW/cm^2 in the UVA region or UV radiation using a 125 W high-pressure mercury lamp (Philips, HPL-N; $\lambda > 290$ nm), with emission bands in the UV region at 304, 314, 335, and 366 nm, maximum emission at 366 nm, and an intensity of 5.304 mW/cm^2, together with an appropriate concave mirror. The radiation energy fluxes were measured using a Delta Ohm HD 2102.2 (Padova, Italy) radiometer fitted with the LP 471 UV (spectral range 315–400 nm) and LP 471 RAD (spectral range 400–1050 nm) sensors. During irradiation, the stirring and streaming with an O_2 constant rate flow were continued. At different time intervals, samples were taken from the cell, and then, the kinetic studies of AMI/ALP photodegradation were monitored via ultrafast liquid chromatography with a UV/Vis diode array detector (UFLC–DAD, Shimadzu Nexera, Tokyo, Japan), set at an appropriate wavelength. The photodegradation samples were first filtered through a Millipore (Millex-GV, Burlington, MA, USA, 0.22 μm) membrane filter in order to remove nanopowders, and then, samples were injected and analyzed with UFLC–DAD. Procedures for UFLC–DAD analysis were described previously [24].

The reusability of ZnO/SnO_2 (synthesized at a molar ratio 2:1 and calcined at 700 °C) in the photodegradation of ALP (0.03 mmol/L) was assessed with catalyst loading of 1.0 mg/mL under SSI. The reutilization was tested for three successive runs using a procedure described previously [25].

3. Results and Discussion

3.1. Characterization of the Photocatalysts

According to the results of SEM analysis (Figure 1), the ZnO 500 and ZnO/SnO_2 (1:1), 500 samples are portrayed by different morphologies in terms of the shape and size of the particles present, as well as their tendency to aggregate. The ZnO sample is composed of irregularly shaped, overlapped particles with smooth edges. Most of them are mutually connected in a way to form grape-like agglomerates implying that the applied annealing temperature was sufficiently high to cause the sintering phenomenon. This is clearly visible based on the shape of the formed aggregates (a few polyhedral particles merged into one aggregate). On the other hand, the ZnO/SnO_2 (1:1), 500 sample was less prone to sintering at the same annealing temperature, which can be confirmed by the smaller size of the formed aggregates and the presence of some individual particles after the calcination. Additionally, it can be suggested that the reduced size of the aggregates in the case of mixed the ZnO/SnO_2 photocatalyst compared to pure ZnO is the consequence of the smaller particles initially present in the sample before the annealing treatment. The results of EDS analysis showed the elemental composition of both samples, verifying the

presence of 86.8 wt% Zn and 13.2 wt% O in ZnO 500 nanopowder, while the mixed binary zinc-tin-oxide sample consists of 33.0 wt% Zn, 46.3 wt% Sn, and 20.7 wt% O.
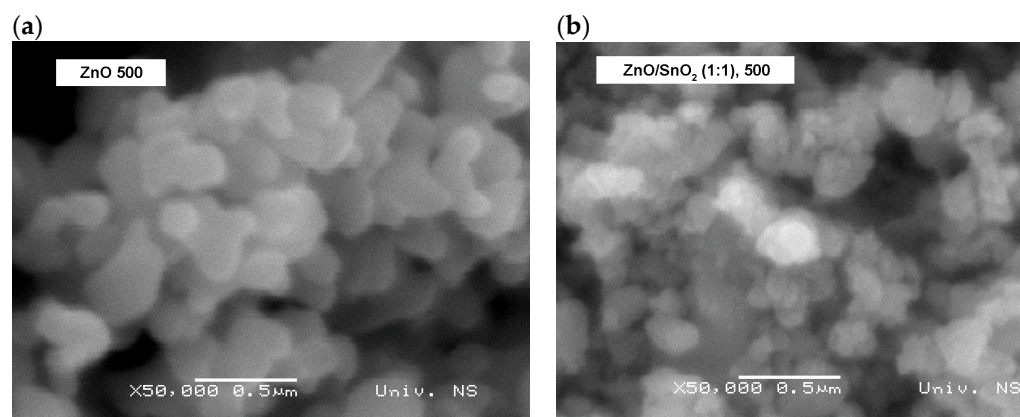
Figure 1. SEM images of the characterized photocatalysts: ZnO 500 (**a**) and ZnO/SnO$_2$ (1:1), 500 (**b**).

The crystal phase composition of the selected photocatalysts was determined based on the XRD analysis (Figure 2). All peaks detected in the ZnO 500 sample are associated with the hexagonal zincite structure with the most intense signals at 2θ values of 31.7° (010), 34.4° (002), and 36.2° (011) (COD database code: 9011662, Reference code 96-901-1663). The average crystallite size was calculated by Scherrer's equation based on the reflection from the (011) plane and amounts to 55.3 nm. In the case of mixed the ZnO/SnO$_2$ photocatalyst, the presence of individual phases of ZnO and SnO$_2$ was found indicating that any additional phase due to their mixing was not observed. The peaks indexed to crystalline tetragonal SnO$_2$ (cassiterite) are located at 2θ values of 26.8° (110), 33.9° (011), and 51.9° (121) (COD database code: 1000062, Reference code 96-100-0063). Evaluating the full-width half-maximum of the characteristic ZnO peak in the pure and binary sample, it can be concluded that the average crystallite size of ZnO is significantly reduced after mixing with SnO$_2$ (19.4 nm). The size of SnO$_2$ nanocrystals was calculated to be 44.8 nm. By comparing the integrated intensities of the diffraction peaks from both phases, their weight fractions were identified semi-quantitatively from the corresponding XRD pattern accounting for 22 wt% of ZnO and 78 wt% of SnO$_2$.

The DLS technique was used to determine the particle size distributions and zeta potentials of two selected photocatalytic nanopowders that proved to be the most effective: ZnO 500 and ZnO/SnO$_2$ (1:1), 500. As can be seen from the diagram shown in Figure 3, both samples are characterized by a monomodal particle size distribution in a wide range of 90–1000 nm for the ZnO sample and 300–1100 nm for the mixed ZnO/SnO$_2$ (1:1), 500 photocatalyst. The average size of pure ZnO particles amounts to 954 nm, while the particles of the mixed oxides can be portrayed by a much smaller average size (284 nm). The peaks that appear on the particle size distribution graph at around 5 μm most likely originate from dust particles or very hard agglomerates, but they have no statistical significance. In accordance with the results of the SEM analysis, it can be concluded that the measured size of the particles for both samples primarily corresponds to aggregates present. The obtained zeta potential of ZnO 500 was 7.2 mV, while the mixing and further annealing with SnO$_2$ resulted in a substantial increase in the zeta potential to 29.7 mV for the binary sample.
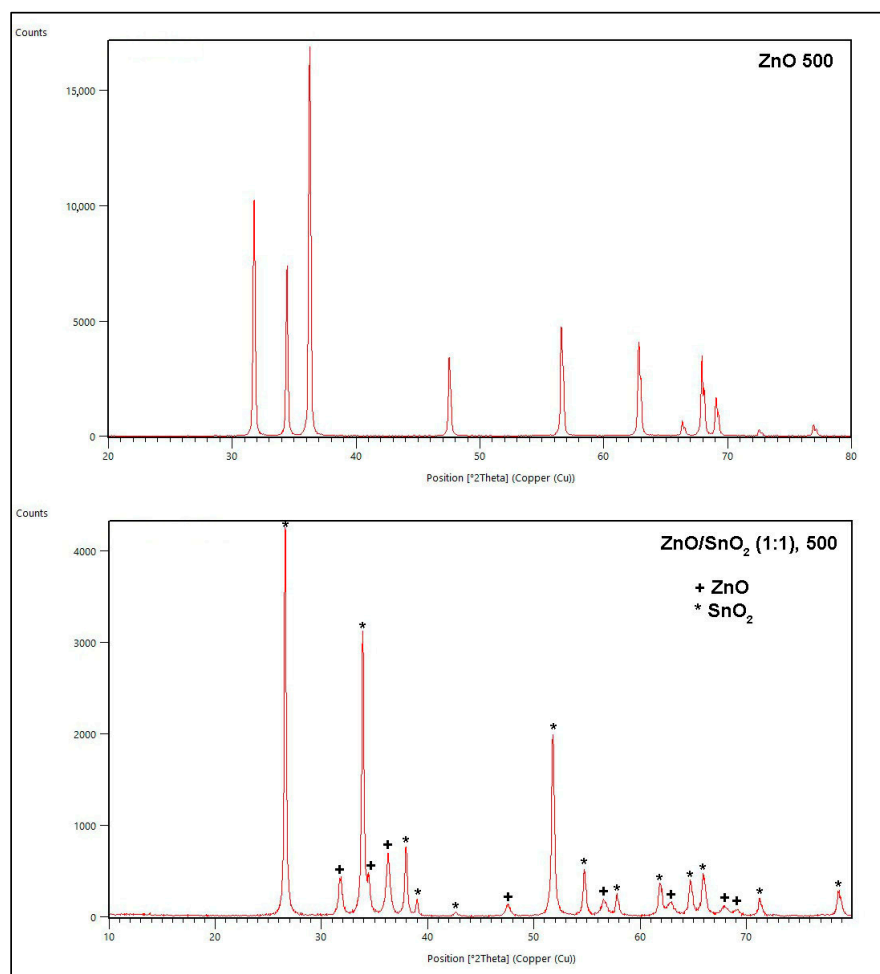
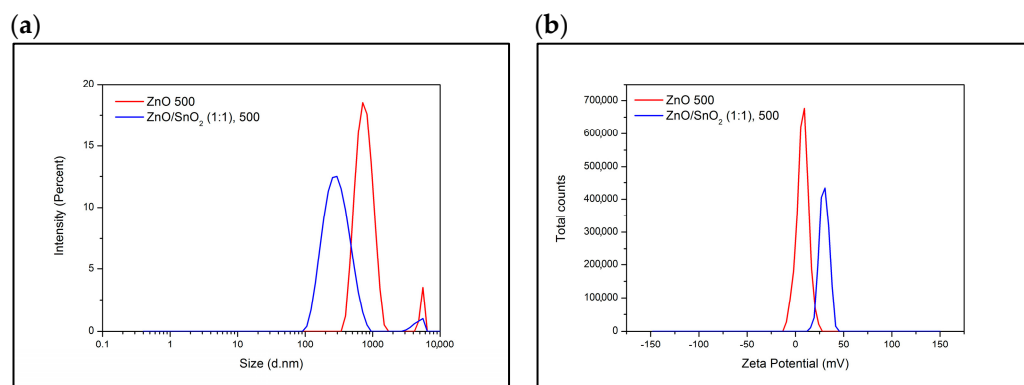**Figure 2.** XRD patterns of the characterized photocatalysts.

Figure 3. Particle size distribution (**a**) and zeta potential distribution (**b**) of the characterized photocatalysts.

Optical absorption spectra for the selected photocatalysts were recorded in the wavelength range 200–800 nm, while the optical band gaps (E_g) were evaluated based on Tauc's relation (Figure 4). The pure ZnO sample is characterized by one wide peak in the absorption spectra with a maximum at 420 nm, while the addition of SnO_2 has shifted this maximum towards lower wavelengths. The binary sample has two absorption maxima, the one of very low intensity at 300 nm and the second one of slightly higher intensity at 375 nm. This photocatalyst exhibited higher absorbance values in the UV region compared to its ZnO counterpart. Although both samples can be related to directly allowed transitions, the values of their corresponding energy gaps differ indicating that the mixing of two

oxides reduces the energy band gap from 3.14 eV (for pure ZnO) to 2.71 eV (for ZnO/SnO$_2$ (1:1), 500).
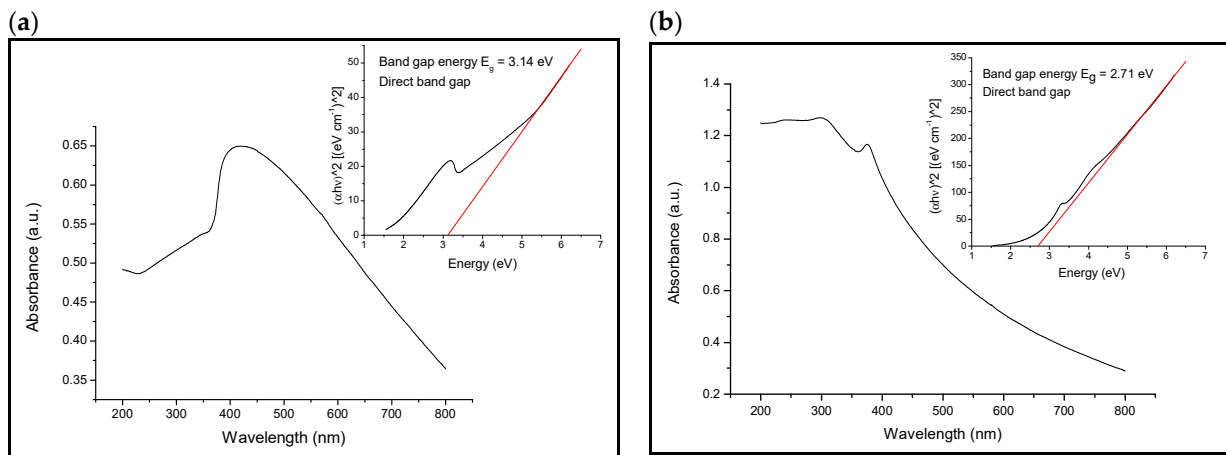
Figure 4. UV/Vis absorption spectra with insets of Tauc's plots showing direct band gap values of ZnO 500 (**a**) and ZnO/SnO$_2$ (1:1), 500 (**b**) samples.
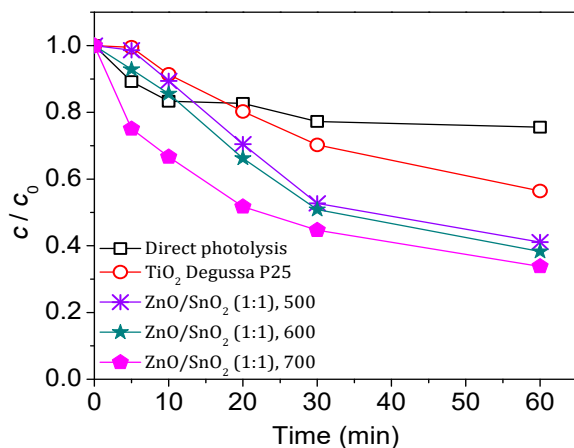
3.2. Efficiency of Photocatalytic Degradation of Amitriptyline

The photocatalytic activity of mixed ZnO/SnO$_2$ photocatalysts was investigated in the photocatalytic degradation of AMI and ALP using UV and SSI. In our previous work, Ivetić et al. [26] examined the efficiency of ZnO/SnO$_2$ (2:1) calcined at 700 °C. In this study, modifications were made regarding the calcination temperature and the ratio of ZnO and SnO$_2$. Figure 5 shows the results of photocatalytic degradation of AMI using ZnO/SnO$_2$ (2:1), calcined at three different temperatures (500, 600, and 700 °C), and based on the obtained results, it can be concluded that the use of mixed photocatalysts increased the degradation efficiency in comparison with degradation results using TiO$_2$ Degussa P25 as a photocatalyst. ZnO/SnO$_2$ (2:1) calcined at 700 °C proved to be the most effective, since 82.6% of AMI was degraded after 60 min of irradiation. This increase in efficiency may be due to a better separation of e$^-$ and h$^+$, i.e., a decrease in charge carrier recombination in the case of mixed binary zinc-tin-oxide nanopowders. In addition, the calcination temperature can have an effect on the size of the photocatalyst particles and therefore on the efficiency of the photocatalytic degradation process [27]. Based on the obtained kinetic curves, a positive effect of increasing the calcination temperature can be seen. Specifically, at 500 °C and 600 °C, the effect of temperature was not very pronounced; however, with an increase in the calcination temperature to 700 °C, the efficiency of the degradation process increased significantly.

In addition to the calcination temperature, the molar ratio of ZnO and SnO$_2$ oxides is a factor that can greatly affect the photocatalytic activity of the photocatalyst. According to this, the photocatalytic degradation of AMI was also investigated using ZnO/SnO$_2$ (1:1) photocatalysts under the same experimental conditions (Figure 6). As can be seen from the Figure 6, the photocatalytic degradation efficiency of AMI using mixed ZnO/SnO$_2$ (1:1) photocatalysts calcined at three different temperatures (500, 600, and 700 °C) was significantly higher than the degradation efficiency using TiO$_2$ Degussa P25. ZnO/SnO$_2$ (1:1) calcined at 700 °C and was found to be most effective, and 66.2% AMI was removed after 60 min of irradiation. Likewise, as in the results presented previously, the direct photolysis of AMI showed the lowest efficiency. Based on the results obtained, the positive effect of a calcination temperature increase on the efficiency of mixed binary nanopowders in the photocatalytic degradation of AMI was evident, although the positive effect was not as pronounced as in the case of ZnO/SnO$_2$ at a molar ratio of 2:1.
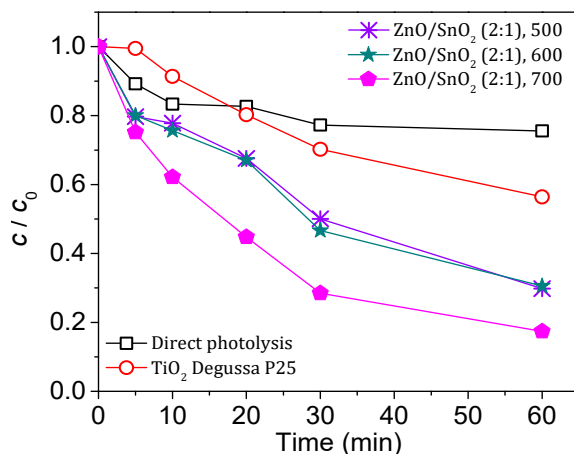
Figure 5. Efficiency of photolytic and photocatalytic degradation of AMI (0.03 mmol/L) using different ZnO/SnO$_2$ (2:1) and TiO$_2$ Degussa P25 (1.0 mg/mL) photocatalysts under SSI.

Figure 6. Efficiency of photolytic and photocatalytic degradation of AMI (0.03 mmol/L) using different ZnO/SnO$_2$ (1:1) and TiO$_2$ Degussa P25 (1.0 mg/mL) photocatalysts under SSI.

In our previous work, Ivetić et al. [26] examined the efficiency of pure ZnO calcined at 700 °C. Additionally, in this work, the influence of calcination temperature (in the temperature range from 500 to 1100 °C) on the efficiency of pure ZnO in photocatalytic degradation of AMI was examined using SSI, and the obtained results are shown in Figure 7.
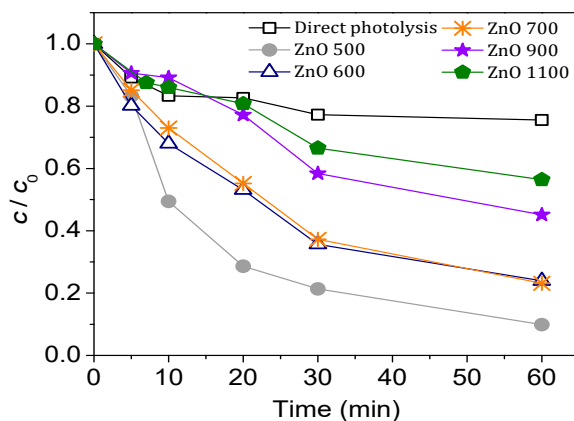

Figure 7. Effect of calcination temperature on the efficiency of ZnO (1.0 mg/mL) in the photocatalytic degradation of AMI (0.03 mmol/L) under SSI.

According to the obtained results, the highest efficiency of AMI removal was achieved using ZnO calcined at 500 °C. Almost the same photocatalytic activity was shown with ZnO nanopowders calcined at 600 and 700 °C, with the fact that in the initial period of degradation, ZnO calcined at 600 °C showed slightly higher photocatalytic activity. In addition, in the presence of ZnO nanopowders calcined at 600 and 700 °C, the efficiency of AMI degradation was decreased compared to that with ZnO calcined at 500 °C, and with a further increase in the calcination temperature to 900 and 1100 °C, the efficiency of AMI degradation dropped significantly. Decreases of the photocatalytic activity of the investigated ZnO nanopowders were probably due to the changes in the morphology and size of the ZnO particles, which were caused by increasing the calcination temperature. A change in the calcination temperature can cause changes in the crystal structure and consequently in the particle size, which is directly related to the specific surface area of the photocatalyst and therefore to its photocatalytic activity [28].

The mixing of two semiconductors generally limiting the crystal growth of both oxides showed that the mean particle sizes of ZnO and SnO_2 are larger in individual oxides than in mixed ZnO/SnO_2 nanopowders at the same calcination temperature, and thus, the specific surface area of mixed oxides is expected to be higher compared to ZnO [29]. Based on the results presented so far, it can be concluded that the positive influence of mixing oxides was observed at a molar ratio of 2:1 and at a calcination temperature of 700 °C.

In order to determine the optimal mass concentration of ZnO/SnO_2 (2:1), 700 °C, the effect of the mass concentration of ZnO/SnO_2 (2:1), 700 °C in the range from 0.1 to 2.0 mg/mL on the kinetics of photocatalytic degradation of AMI (Figure 8) was investigated. Based on the obtained results, it can be concluded that the optimal mass concentration of the photocatalyst is 1.0 mg/mL. With an increase in the mass concentration of the photocatalyst, the efficiency of the AMI degradation process increased up to 1.0 mg/mL, and after that, at a catalyst loading of 2.0 mg/mL, the efficiency of the degradation process showed decreasing trend.
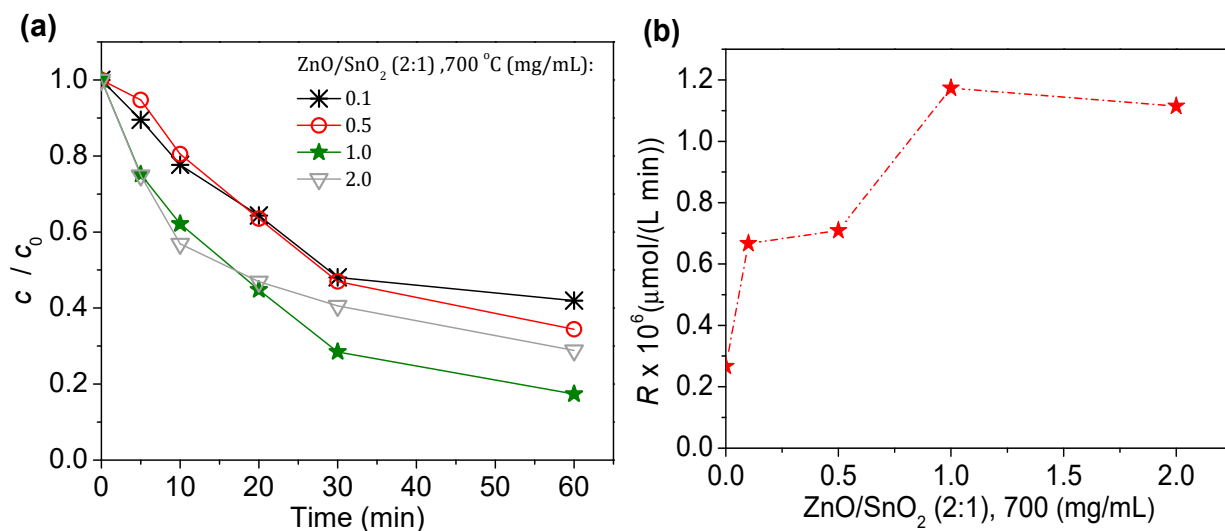

Figure 8. The influence of the ZnO/SnO_2 (2:1), 700 loading on the efficiency of the photocatalytic degradation of AMI (0.03 mmol/L) (**a**) and the dependence of the degradation rate on photocatalyst loading, calculated for the first 20 min of irradiation (**b**).

3.3. Efficiency of Photocatalytic Degradation of Alprazolam

In order to examine the influence of the substrate type, the efficiency of the synthesized mixed ZnO/SnO_2 photocatalysts, in addition to the photocatalytic degradation of AMI, was also tested for the photocatalytic degradation of ALP. The photocatalytic efficiency of ZnO/SnO_2 (2:1) photocatalyst calcinations at three different temperatures (500, 600, and 700 °C) was tested (Figure 9). Based on the obtained results, the conclusion is that mixed

ZnO/SnO$_2$ (2:1) photocatalysts showed better photocatalytic activity compared to the results obtained using TiO$_2$ Degussa P25. In addition, it can be seen that with an increase in the calcination temperature, substrate removal efficiency increases to a small extent, and ZnO/SnO$_2$ (2:1) calcined at 700 °C turned out to be the most effective, where 77.5% of ALP was degraded after 60 min of irradiation. Likewise, if the results of the photocatalytic degradation of AMI (Figure 5) are compared with the results of ALP degradation (Figure 9), ZnO/SnO$_2$ (2:1) calcined at 500 °C showed almost the same activity in the photocatalytic degradation of both substrates; slightly higher degradation efficiency of ALP was achieved using ZnO/SnO$_2$ (2:1) calcined at 600 °C, while ZnO/SnO$_2$ (2:1) calcined at 700 °C proved to be more effective in AMI degradation.
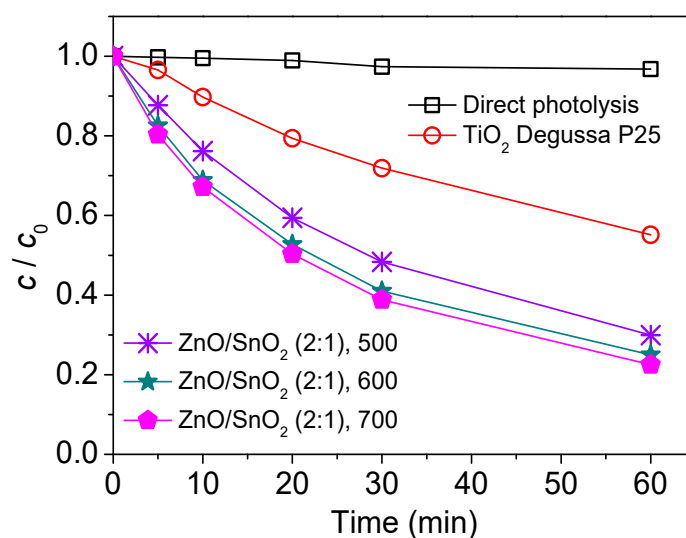

Figure 9. Efficiency of photolytic and photocatalytic degradation of ALP (0.03 mmol/L) in the presence of different ZnO/SnO$_2$ (2:1) and TiO$_2$ Degussa P25 as photocatalysts (1.0 mg/mL) under SSI.

Moreover, the efficiency of the photocatalytic degradation of ZnO/SnO$_2$ (1:1) was examined, with the aim of studying the influences of the molar ratios of the starting oxides ZnO and SnO$_2$ on the efficiency of ALP removal (Figure 10). As can be seen, mixed ZnO/SnO$_2$ (1:1) showed significantly higher efficiency in the photocatalytic degradation of ALP compared to TiO$_2$ Degussa P25. The influence of the calcination temperature was less pronounced, compared to the influence that the calcination temperature had in the case of the ZnO/SnO$_2$ (2:1) photocatalysts. Nevertheless, among investigated ZnO/SnO$_2$ (1:1), nanomaterial calcined at 700 °C proved to be the most effective, and with its application, 74.6% of ALP was removed after 60 min of irradiation. If the results of the photocatalytic degradation of AMI (Figure 6) and ALP (Figure 10) are compared, it can be seen that all tested ZnO/SnO$_2$ (1:1) showed slightly higher photocatalytic activity in the degradation of ALP using SSI. The obtained differences in the efficiencies of the applied photocatalysts for the removal of two different substrates indicated the importance of the investigated effects.

As in the case of AMI, the efficiencies of the photocatalytic degradation of ALP were tested using pure ZnO, calcined at different temperatures (Figure 11). Based on the presented results, it can be concluded that, as in the case of the photocatalytic degradation of AMI, the photocatalytic efficiency of the tested ZnO decreases with an increase in the calcination temperature. Likewise, comparing the results of the photocatalytic decomposition of AMI (Figure 7) and ALP (Figure 11), it can be concluded that calcined ZnO prepared at all calcination temperatures showed slightly higher photocatalytic activity in the degradation of AMI.
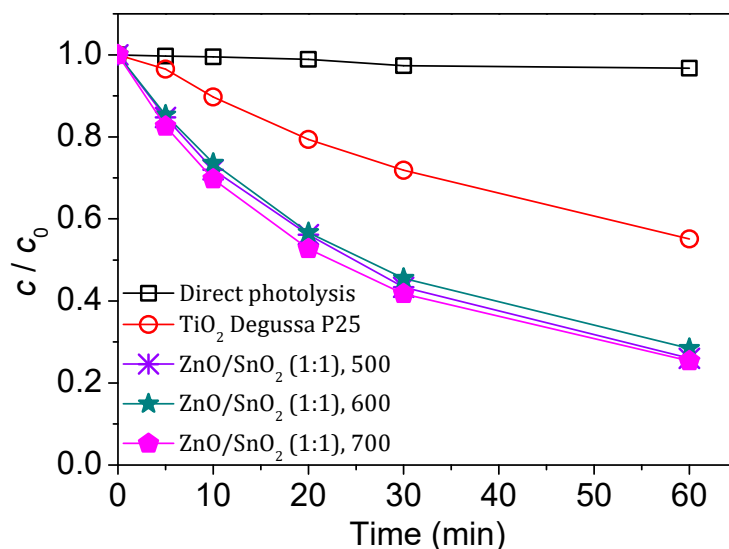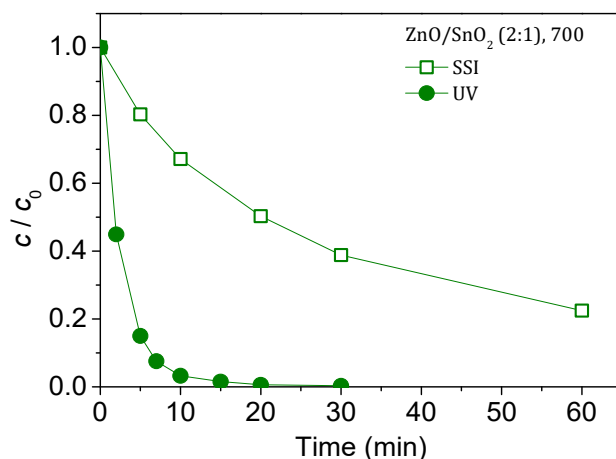
Figure 10. Efficiency of photolytic and photocatalytic degradation of ALP (0.03 mmol/L) in the presence of different ZnO/SnO$_2$ (1:1) and TiO$_2$ Degussa P25 photocatalysts (1.0 mg/mL) under SSI.
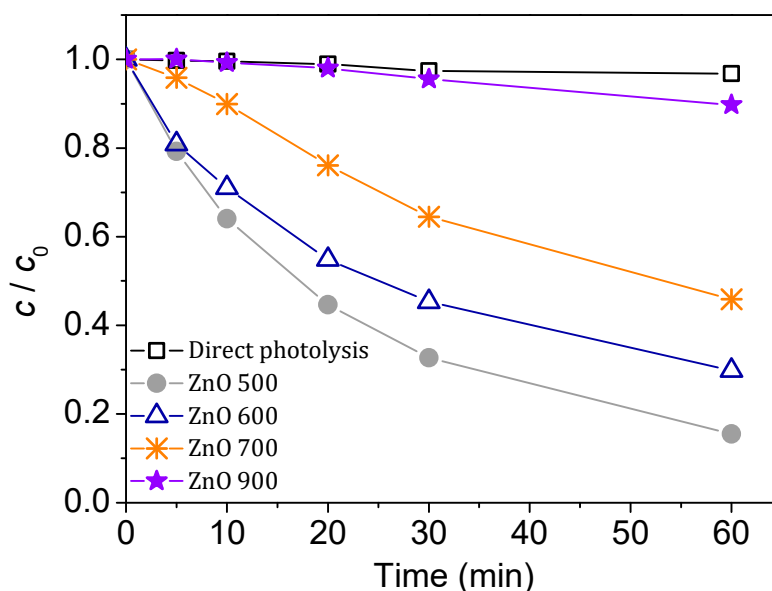

Figure 11. The influence of calcination temperature on the efficiency of ZnO (1.0 mg/mL) in the photocatalytic degradation of ALP (0.03 mmol/L) using SSI.

Generally, the results of the photocatalytic degradation of ALP show that at a calcination temperature of 500 °C, the oxide mixing procedure reduced the efficiency of ALP degradation. At 600 °C, a positive effect of mixing was already observed, while a more pronounced positive effect of mixing ZnO and SnO$_2$ was found at a calcination temperature of 700 °C. Given that in the case of the ALP removal process, ZnO/SnO$_2$ (2:1), 700 proved to be the most effective, the influence of the type of radiation on the efficiency of the photocatalytic degradation of ALP was examined using UV and SSI, and the obtained results are shown in Figure 12. As can be seen, by applying UV irradiation, ALP was completely removed after 30 min of the removal process. However, with the application of SSI, satisfactory efficiency was also achieved, which is very significant from an economic point of view and for the applicability of the system under real-life conditions.

Figure 12. Influence of radiation type on the efficiency of photocatalytic degradation of ALP (0.03 mmol/L) in the presence of ZnO/SnO$_2$ (2:1), 700 (1.0 mg/mL) as photocatalyst.

Similarly, the influence of the mass concentrations of ZnO/SnO$_2$ (2:1), 700 ranging from 0.5 to 5.0 mg/mL on the kinetics of the photocatalytic degradation of ALP by SSI were examined (Figure 13).
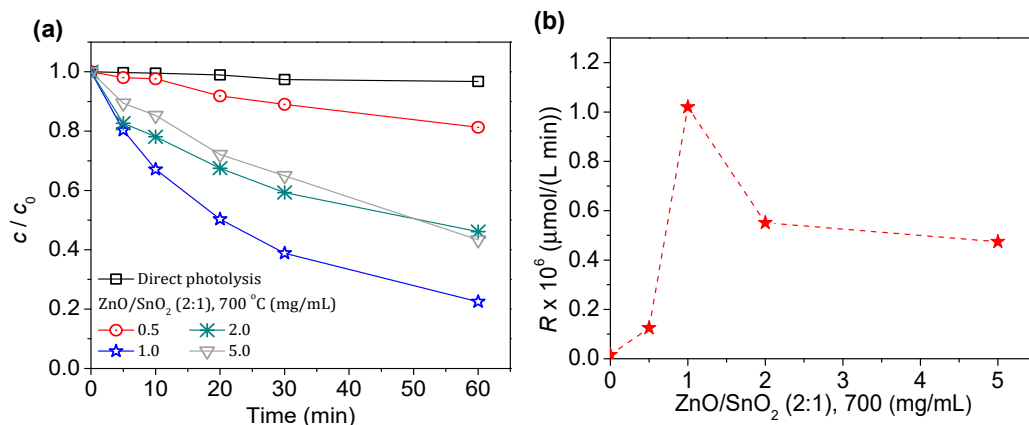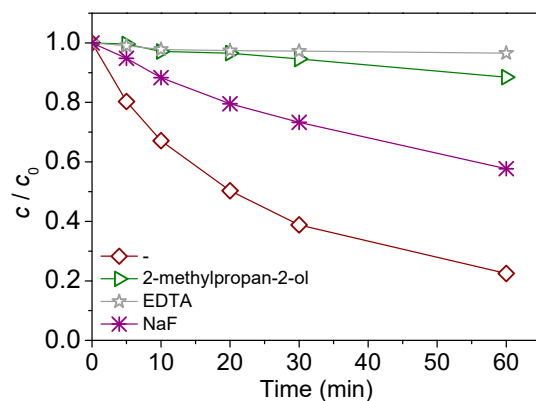

Figure 13. The influence of the ZnO/SnO$_2$ (2:1), 700 loading on the efficiency of the photocatalytic degradation of ALP (0.03 mmol/L) (**a**) and the dependence of the degradation rate on the photocatalyst loading, calculated for the first 20 min of irradiation (**b**).

From the presented results, it can be concluded that the optimal mass concentration of the photocatalyst was 1.0 mg/mL. Namely, with an increase in the mass concentration, the efficiency of the degradation process increases up to 1.0 mg/mL, and after that, at the mass concentration of 2.0 and 5.0 mg/mL, the efficiency of the ALP removal significantly decreased.

We determined that the highest photodegradation efficiency had been reached in the case of ZnO/SnO$_2$ synthesized at a molar ratio of 2:1 and calcined at 700 °C, under 1.0 mg/mL catalyst loading, so we also performed a reutilization study to examine the recycling efficiency of the abovementioned photocatalyst. The experiments were conducted in three successive runs, while keeping the experimental conditions unchanged. The obtained findings showed that there was no loss of the photocatalytic capability observed with the ZnO/SnO$_2$ catalyst, synthesized at a molar ratio of 2:1 and calcined at 700 °C. The removal efficiency after 60 min of photodegradation in each run was unchanged (~60%) and stayed effective after being investigated for three uses

Finally, in order to assume the possible mechanism of the photocatalytic degradation of ALP in the presence of the photocatalyst ZnO/SnO$_2$ (2:1), 700 using SSI, experiments on the photocatalytic degradation of ALP with the addition of radical/hole scavengers were performed. As the $^\bullet$OH radical scavenger 2-methylpropan-2-ol was used, NaF was

used in order to examine the influence of adsorbed $^\bullet$OH radicals on the efficiency of the photocatalytic degradation of ALP, as well as EDTA as a hole scavenger. The obtained results shown in Figure 14 indicated that the inhibition of ALP photocatalytic degradation was established in the presence of all tested scavengers, but the percentage of inhibition was different. The addition of EDTA led to complete inhibition of the photocatalytic degradation of ALP, indicating that the degradation was predominantly proceeded by the reaction with holes. Inhibition in the presence of 2-methylpropan-2-ol and NaF indicated that the decomposition also takes place through the reaction with $^\bullet$OH radicals, mainly via free $^\bullet$OH radicals.

Figure 14. The influence of radical/hole scavengers (1.0 mmol/L) on the efficiency of photocatalytic degradation of ALP (0.03 mmol/L) in the presence of ZnO/SnO_2 (2:1), 700 (1.0 mg/mL) as a photocatalyst under SSI.

4. Conclusions and Outlooks

In this research, the efficiency of the synthesized, coupled, binary ZnO-based nanoparticles (ZnO/SnO_2) were investigated under different experimental conditions as nanopowders. They were synthesized using a solid-state method, at both 2:1 and 1:1 molar ratios, and calcined at different temperatures.

To begin, the effects of calcination temperatures on the efficiency of ZnO/SnO_2 nanoparticles were examined for the removal of AMI and ALP. Our observations indicate that at both molar ratios, the highest removal rate was reached in the presence of nanoparticles calcined at 700 °C. Both molar ratios of binary ZnO/SnO_2 showed a higher efficiency than TiO_2 Degussa P25. However, the 2:1 molar ratio showed higher activity in the removal of AMI and ALP than 1:1. Hence, further experiments were carried out in the presence of ZnO/SnO_2 (2:1). Furthermore, since the catalyst loading is one of the most important photocatalytic factors, experiments were carried out in favor of determining its effect on the photodegradation of AMI and ALP in the presence of ZnO/SnO_2 (2:1). The investigated pollutants showed similar behavior. In both cases, the 1.0 mg/mL catalyst loading has proven to be the best. Moreover, the effect of the irradiation type was also investigated in the case of ALP. As expected, the highest efficiency was achieved under UV irradiation. However, it must be highlighted that under SSI, satisfactory results were also achieved, which is essential for practical uses of photocatalytic degradation, i.e., under natural conditions.

Additionally, the pure ZnO powder calcined at various temperatures (500–1100 °C) was also examined in the heterogeneous photocatalysis of AMI and ALP. In the case of both examined pollutants, the highest efficiency was reached in the presence of ZnO calcined at 500 °C.

The obtained photocatalytic results were further confirmed based on the characterization data. Namely, due the lower bandgap energy in the case of ZnO/SnO_2 (1:1), 500 and because of the lower particle aggregation proven by SEM and DLS, a higher photocatalytic activity was expected, compared to that with pure ZnO.

Finally, our findings obtained in the presence of ALP and *tert*-butanol, NaF, and EDTA suggested that the relative contribution of various reactive species changed in the following order: positively charged holes > $OH^{\bullet}_{free}$ > $OH^{\bullet}_{ads}$. In the future, more emphasis should be put on improvements in the newly synthesized binary coupled ZnO/SnO_2 nanoparticles. By doing this, we may be able to obtain a semiconductor that possesses higher photocatalytic activity under solar irradiation. This is crucial, since solar irradiation is a free and renewable source of energy, which should be exploited instead of using costly radiation sources. Furthermore, the toxicity of the mentioned pollutants and their photodegradation intermediates should also be examined in detail. In this way, we would obtain more information about the effect of AMI and ALP on the living organisms and encourage actions to be taken in favor of environmental protection. Last but not least, some green approaches, for instance plant extracts, should be also investigated in the synthesis of the mentioned nanoparticles. By doing this, we could further reduce the costs of chemicals and most importantly reduce our footprint in the environment and make the heterogeneous photocatalysis more sustainable, affordable, and widespread.

Author Contributions: Conceptualization, N.F. and B.A.; methodology, N.F., S.P. and T.I.; validation, N.F., V.D. and N.B.; formal analysis, N.F., S.B., D.J. and S.P.; investigation, N.F., S.B., D.J., S.P. and T.I.; resources, T.I.; data curation, N.F., V.D., N.B. and S.P.; writing—original draft preparation, N.F., D.Š.M., V.D., N.B., S.B., D.J. and S.P.; writing—review and editing, N.F., D.Š.M., P.P. and B.A.; supervision, D.Š.M. and B.A. All authors have read and agreed to the published version of the manuscript.

Data Availability Statement: Not applicable.

Conflicts of Interest: The authors declare no conflict of interest. The funders had no role in the design of the study; in the collection, analyses, or interpretation of data; in the writing of the manuscript; or in the decision to publish the results.

References

1. Kotrotsiou, O.; Kiparissides, C. Water Treatment by Molecularly Imprinted Materials. In *Nanoscale Materials in Water Purification*; Elsevier: Oxford, UK, 2019; pp. 179–230.
2. Schoeman, C.; Dlamini, M.; Okonkwo, O.J. The impact of a Wastewater Treatment Works in Southern Gauteng, South Africa on efavirenz and nevirapine discharges into the aquatic environment. *Emerg. Contam.* **2017**, *3*, 95–106. [CrossRef]
3. Peng, Y.; Fang, W.; Krauss, M.; Brack, W.; Wang, Z.; Li, F.; Zhang, X. Screening hundreds of emerging organic pollutants (EOPs) in surface water from the Yangtze River Delta (YRD): Occurrence, distribution, ecological risk. *Environ. Pollut.* **2018**, *241*, 484–493. [CrossRef] [PubMed]
4. Puckowski, A.; Mioduszewska, K.; Lukaszewicz, P.; Borecka, M.; Caban, M.; Maszkowska, J.; Stepnowski, P. Bioaccumulation and analytics of pharmaceutical residues in the environment: A review. *J. Pharm. Biomed. Anal.* **2016**, *127*, 232–255. [CrossRef] [PubMed]
5. Miller–Keane Encyclopedia and Dictionary of Medicine, Nursing, and Allied Health, Seventh Edition, Saunders, Elsevier, Inc. 2003. Available online: https://medical-dictionary.thefreedictionary.com/antidepressant (accessed on 23 November 2022).
6. Grung, M.; Heimstad, E.S.; Moe, M.; Schlabach, M.; Svenson, A.; Thomas, K.; Woldegiorgis, A. *Human and Veterinary Pharmaceuticals, Narcotics, and Personal Care Products in the Environment (Report 2325/2007)*; Statens Forurensningstilsyn: Oslo, Norway, 2007; pp. 30, 36, 47–48, 88–91. Available online: https://www.miljodirektoratet.no/globalassets/publikasjoner/klif2/publikasjoner/2325/ta2325.pdf (accessed on 23 November 2022).
7. Calisto, V.; Domingues, M.R.; Esteves, V.I. Photodegradation of psychiatric pharmaceuticals in aquatic environments—Kinetics and photodegradation products. *Water Res.* **2011**, *45*, 6097–6106. [CrossRef] [PubMed]
8. Mezzelani, M.; Gorbi, S.; Regoli, F. Pharmaceuticals in the aquatic environments: Evidence of emerged threat and future challenges for marine organisms. *Mar. Environ. Res.* **2018**, *140*, 41–60. [CrossRef] [PubMed]
9. Alvarez-Freire, I.; Brunetti, P.; Cabarcos-Fernandez, P.; Fernandez-Liste, A.; Tabernero-Duque, M.J.; Bermejo-Barrera, A.M. Determination of benzodiazepines in pericardial fluid by gas chromatography-mass spectrometry. *J. Pharm. Biomed. Anal.* **2018**, *159*, 45–52. [CrossRef] [PubMed]
10. Romeiro, A.; Freitas, D.; Emilia Azenha, M.; Canle, M.; Burrows, H.D. Effect of the calcination temperature on the photocatalytic efficiency of acidic sol-gel synthesized TiO(2) nanoparticles in the degradation of alprazolam. *Photochem. Photobiol. Sci.* **2017**, *16*, 935–945. [CrossRef]

11. Richardson, M.L.; Bowron, J.M. The fate of pharmaceutical chemicals in the aquatic environment. *J. Pharm. Pharmacol.* **1985**, *37*, 1–12. [CrossRef]

12. Mahy, J.G.; Wolfs, C.; Mertes, A.; Vreuls, C.; Drot, S.; Smeets, S.; Dircks, S.; Boergers, A.; Tuerk, J.; Lambert, S.D. Advanced photocatalytic oxidation processes for micropollutant elimination from municipal and industrial water. *J. Environ. Manag.* **2019**, *250*, 109561. [CrossRef]

13. Chatzitakis, A.; Berberidou, C.; Paspaltsis, I.; Kyriakou, G.; Sklaviadis, T.; Poulios, I. Photocatalytic degradation and drug activity reduction of Chloramphenicol. *Water. Res.* **2008**, *42*, 386–394. [CrossRef] [PubMed]

14. Chen, J.; Ray, A.K. Photocatalytic kinetics of phenol and its derivatives over UV irradiated TiO_2. *Appl. Catal. B* **1999**, *23*, 143–157. [CrossRef]

15. Kumar, S.; Ahlawat, W.; Bhanjana, G.; Heydarifard, S.; Nazhad, M.M.; Dilbaghi, N. Nanotechnology-based water treatment strategies. *J. Nanosci. Nanotechnol.* **2014**, *14*, 1838–1858. [CrossRef] [PubMed]

16. Li, J.; Wu, N. Semiconductor-based photocatalysts and photoelectrochemical cells for solar fuel generation: A review. *Catal. Sci. Technol.* **2015**, *5*, 1360–1384. [CrossRef]

17. Wang, H.; Baek, S.; Lee, J.; Lim, S. High photocatalytic activity of silver-loaded ZnO-SnO_2 coupled catalysts. *Chem. Eng. J.* **2009**, *146*, 355–361. [CrossRef]

18. Liu, C.; Mao, S.; Wang, H.; Wu, Y.; Wang, F.; Xia, M.; Chen, Q. Peroxymonosulfate-assisted for facilitating photocatalytic degradation performance of 2D/2D WO_3/BiOBr S-scheme heterojunction. *Chem. Eng. J.* **2022**, *430*, 132806. [CrossRef]

19. Liu, C.; Mao, S.; Shi, M.; Hong, X.; Wang, D.; Wang, F.; Xia, M.; Chen, Q. Enhanced photocatalytic degradation performance of BiVO4/BiOBr through combining Fermi level alteration and oxygen defect engineering. *Chem. Eng. J.* **2022**, *449*, 137757. [CrossRef]

20. Liu, C.; Mao, S.; Shi, M.; Wang, F.; Xia, M.; Chen, Q.; Ju, X. Peroxymonosulfate activation through 2D/2D Z-scheme CoAl-LDH/BiOBr photocatalyst under visible light for ciprofloxacin degradation. *J. Hazard. Mater.* **2021**, *420*, 126613. [CrossRef]

21. Zhu, B.; Cheng, B.; Fan, J.; Ho, W.; Yu, J. g-C_3N_4-based 2D/2D composite heterojunction photocatalyst. *Small Struct.* **2021**, *2*, 2100086. [CrossRef]

22. Bie, C.; Yu, H.; Cheng, B.; Ho, W.; Fan, J.; Yu, J. Design, Fabrication, and Mechanism of Nitrogen-Doped Graphene-Based Photocatalyst. *Adv. Mater.* **2021**, *33*, e2003521. [CrossRef]

23. Tomić, N.; Grujić-Brojčin, M.; Finčur, N.; Abramović, B.; Simović, B.; Krstić, J.; Matović, B.; Šćepanović, M. Photocatalytic degradation of alprazolam in water suspension of brookite type TiO_2 nanopowders prepared using hydrothermal route. *Mater. Chem. Phys.* **2015**, *163*, 518–528. [CrossRef]

24. Finčur, N.L.; Šćepanović, M.J.; Grujić-Brojčin, M.; Abramović, B.F.; Krstić, J.B.; Kremenović, A.; Srećković, T.; Golubović, A. Adsorption and degradation of some psychiatric drugs by sol-gel synthesized titania-based photocatalysts: Influence of tungsten and sodium content. *J. Sol-Gel Sci. Technol.* **2019**, *90*, 510–524. [CrossRef]

25. Finčur, N.L.; Krstić, J.B.; Šibul, F.S.; Šojić, D.V.; Despotović, V.N.; Banić, N.D.; Agbaba, J.R.; Abramović, B.F. Removal of alprazolam from aqueous solutions by heterogeneous photocatalysis: Influencing factors, intermediates, and products. *Chem. Eng. J.* **2017**, *307*, 1105–1115. [CrossRef]

26. Ivetić, T.B.; Finčur, N.L.; Abramović, B.F.; Dimitrievska, M.; Štrbac, G.R.; Čajko, K.O.; Miljević, B.B.; Đačanin, L.R.; Lukić-Petrović, S.R. Environmentally friendly photoactive heterojunction zinc tin oxide nanoparticles. *Ceram. Int.* **2016**, *42*, 3575–3583. [CrossRef]

27. Pardeshi, S.K.; Patil, A.B. Effect of morphology and crystallite size on solar photocatalytic activity of zinc oxide synthesized by solution free mechanochemical method. *J. Mol. Catal. A Chem.* **2009**, *308*, 32–40. [CrossRef]

28. Ahmed, S.; Rasul, M.G.; Martens, W.N.; Brown, R.; Hashib, M.A. Heterogeneous photocatalytic degradation of phenols in wastewater: A review on current status and developments. *Desalination* **2010**, *261*, 3–18. [CrossRef]

29. Hamrouni, A.; Moussa, N.; Parrino, F.; Di Paola, A.; Houas, A.; Palmisano, L. Sol–gel synthesis and photocatalytic activity of ZnO–SnO_2 nanocomposites. *J. Mol. Catal. A Chem.* **2014**, *390*, 133–141. [CrossRef]